Physica B 515 (2017) 8–17

Contents lists available at ScienceDirect

Physica B

journal homepage: www.elsevier.com/locate/physb

Design and fabrication of dioxyphenylcoumarin substituted cyclotriphosphazene compounds photodiodes

Elsayed Elgazzar[a], A. Dere[b], Furkan Özen[c], Kenan Koran[c], Abdullah G. Al-Sehemi[d,e,f], Ahmed A. Al-Ghamdi[g], Ahmet Orhan Görgülü[c], F. El-Tantawy[a], F. Yakuphanoglu[b,*]

[a] Department of Physics, Faculty of Science, Suez Canal University, Ismailia, Egypt
[b] Department of Physics, Faculty of Science, Fırat University, Elazığ, Turkey
[c] Department of Chemistry, Faculty of Science, Fırat University, Elazığ, Turkey
[d] Department of Chemistry, Faculty of Science, King Khalid University, P.O. Box 9004, Abha 61413, Saudi Arabia
[e] Research Center for Advanced Materials Science, King Khalid University, P.O. Box 9004, Abha 61413, Saudi Arabia
[f] Unit of Science and Technology, Faculty of Science, King Khalid University, P.O. Box 9004, Abha 61413, Saudi Arabia
[g] Department of Physics, Faculty of Science, King Abdulaziz University, Jeddah, Saudi Arabia

ARTICLE INFO

Keywords:
Photodiode, Sensor, Cyclotriphosphazene
Dioxycoumarin-phosphazene

ABSTRACT

The present study introduces cyclotriphosphazene compounds substituted by dioxyphenylcoumarin as a photodiode application. Firstly, 7,8-dihydroxy-3-(3-methylphenyl)coumarin (**1b**) has been obtained by conventional as well as microwave assisted methods. Novel optoelectronic device characteristics for both mono and disubstituted dioxyphenylcoumarin bearing cyclotriphosphazene compounds (**HCP-2** and **HCP-4**) have been synthesized from the reactions of cyclotriphosphazene containing dioxybiphenyl **(HCP-1** and **HCP-3)** with compound **1b**, respectively. The structures of compounds **HCP 1–4** were identified by using elemental analysis, ^{1}H, ^{13}C-APT, ^{31}P NMR and 2D HETCOR NMR and FT-IR spectroscopy methods. The Al/HCP-2/p-Si/Al and Al/HCP-4/-p-Si/Al photodiodes properties have been investigated from current-voltage (I – V) and capacitance-voltage (C – V) measurements. The electrical parameters of the prepared diodes such as ideality factor n and series resistance R_s were investigated in dark and at room temperature from (I – V) curve and Nord's method. As can be seen, the Al/HCP-2/p-Si/Al diode of high rectification ratio *RR* and with ideality factor greater than unity. The influence of light illuminations on the diode shows that the device can be used as photodiode with good efficiency. The barrier height ϕ_b and series resistance R_s have been calculated from the capacitance-voltage (C – V)and conductance-voltage (G – V) measurements under various applied frequencies from 10 kHz to 1 MHz. the high difference in the results of barrier height obtained from I-V and C-V calculations confirm the influence of series resistance and localized states on transport of charge carriers and the photodiode performance.

1. Introduction

Phosphazene derivatives are a class of cyclic and polymeric molecules which contain alternating phosphorus and nitrogen atoms bound by alternating single and double bonds in their skeleton [1]. Substituted cyclophosphazenes with phosphorus-carbon bonds have been synthesized from hexacyclotriphosphazenes by Friedel Crafts substitutions and by reactions with nucleophiles such as primary, secondary amines, aryloxides or alkoxides reagents [2–4]. One of the most important property for cyclophosphazene compounds and its derivatives is the substitution reactions exchange between organic groups and phosphorus atoms. Cyclophosphazenes with nucleophilic substitution reactions have several advantages with high thermal and chemical stability. When organic groups are bonded at each phosphorus atom, the phosphazene skeleton is stabilized against hydrolytic attack [1,5]. The phosphazenes, particularly the substituted phosphazene derivatives containing organic or inorganic side groups, have generated considerable research interest in recent years because of their unusual physical and chemical properties such as organic light emitting diodes and fluorescence sensor [6–8], cathode material for rechargeable lithium batteries [9] and flame retardants [10].

In this research we study the cyclotriphosphazene compounds as a new photoconducting material. Although some novel cyclotriphosphazene structures and their physical properties have been reported [11–

* Corresponding author.
E-mail address: fyhan@hotmail.com (F. Yakuphanoglu).

http://dx.doi.org/10.1016/j.physb.2017.03.025
Received 1 March 2017; Received in revised form 15 March 2017; Accepted 16 March 2017
Available online 19 March 2017

14], there is no study about the optoelectronic properties of the cyclotriphosphazene compounds bearing dioxyphenylcoumarin groups. The aim of this work is to determine how the photodiode prepared from both mono and di substituted dioxyphenylcoumarin bearing cyclotriphosphazene compounds (**HCP-2** and **HCP-4**) change and how its characteristics alter regarding with the number of coumarin attachment.

2. Experimental techniques

2.1. Materials and methods

$N_3P_3Cl_6$ (HCP) was provided from TCI and was used by the recrystallization from n-hexane. The 2,2′-dihydroxybiphenyl and cesium carbonate have been procured from Merck and Sigma Aldrich, respectively. All the organic solvents used in the synthesis and purification of the compounds were provided from Merck.

^{1}H, ^{13}C and ^{31}P NMR spectra were recorded in dimethylsulphoxide-d_6 and chloroform-d solutions on a Bruker DPX 400 MHz spectrometer using TMS (an internal reference for ^{1}H NMR) and 85% H_3PO_4 (an external reference for ^{31}P NMR). The micro analysis and FT-IR spectra of compounds were measured using a Leco 932 CHNS-O apparatus and on Perkin Elmer FT-IR spectrometer, respectively.

2.2. Synthesis

2-(2,3,4-trimethoxyphenyl)-1-(3-(methylphenyl))acrylonitrile **(1a)** was synthesized and purified according to methods in the literature [15–17]. Cyclotriphosphazene compounds containing dioxybiphenyl **HCP-1** and **HCP-3** were synthesized as defined by Carriedo et al. [18,19].

2.2.1. Synthesis of 7,8-dihydroxy-3-(3-methylphenyl)coumarin (1b)

A sealed vessel containing a mixture of 2-(2,3,4-trimethoxyphenyl)-1-(3-(methylphenyl))acrylonitrile **(1a)** (0.4 g, 1.3 mmol), an appropriate silica gel (15 g) and pyridinium hydrochloride (5 g) was stirred under argon atmosphere. The reaction was continued for 25 min at 320 W under microwave irradiation. After cooling to room temperature, it was treated with acidified with 1 M HCl (150 mL) and then the product was isolated by filtration. The product was dissolved in acetone (3×30 mL) and it was isolated with using filtration through silica gel. The solvent was evaporated on a rotary evaporator. The solid washed with water many times and then dried under vacuum. The crude product was resolved in ethyl acetate (15 mL) and precipitated with n-hexane (250 mL). The crude solid was purified to column chromatography using chloroform:hexane and the target product **1b** was obtained as a grey solid. Yield=75% (0.26 g). Anal. Calc. for $C_{16}H_{12}O_4$ (MW: 268.26): C, 71.64; H, 4.51; Found C, 71.62; H, 4.50%. FT-IR (KBr, cm^{-1}): 3477, 3316 ν_{O-H}, 3052 $\nu_{C-H(Ar)}$, 2917, 2857 $\nu_{C-H(Al)}$,1676 $\nu_{C=O}$, 1610, 1589, 1509 $\nu_{C=C}$. ^{1}H NMR (400 MHz, DMSO-d_6): δ 2.27 (3H, s, H^{18}), 6.86 (1H, *d*, *J*=8.4 Hz, H^4), 7.13 (1H, *d*, *J*=8.4, H^5), 7.21 (1H, *d*, *J*=7.2 Hz, H^{17}), 7.33 (1H, t, *J*=7.6 Hz, H^{16}), 7.53 (1H, d, *J*=8.8 Hz, H^{15}), 7.55 (1H, s, H^{13}), 8.11 (1H, s, H^9), 9.44 (1H, s, H^7), 10.17 (1H, s, H^8). ^{13}C NMR (400 MHz, DMSO-d_6): δ 21.19 C^{18}, 113.16 C^6, 113.28 C^4, 119.89 C^5, 122.71 C^{10}, 125.64 C^{13}, 128.57 C^{15}, 129.02 C^{17}, 129.23 C^{16}, 131.61 C^{12}, 134.99 C^{14}, 138.01 C^2, 142.06 C^9, 143.08 C^1, 149.20 C^3, 161.17 C^{11}.

2.2.2. Synthesis procedure of 2,2-bis[spiro(7,8-dioxy-3-(3-methylphenyl)coumarin)]-4,4,6,6-bis[spiro(2′,2"-dioxy-1′,1"-biphenylyl)]cyclotriphosphazene (HCP-2)

HCP-1 (0.3 g, 0.52 mmol) and Na_2CO_3 (0.44 g, 4.16 mmol) were dissolved in 50 mL of dry xylene (mixture of isomers) in a 150 mL three-necked reaction flask. 7,8-dihydroxy-3-(3-methylphenyl)coumarin **(1b)** (0.28 g, 1.04 mmol) in 25 mL of xylene was slowly added to the stirred solution at 0 °C. After the reaction mixture was continued for 25 min at 0 °C, it was refluxed in xylene for 48 h. After stopping the reaction, the mixture was filtered to separate the formed sodium chloride. Xylene was evaporated at rotary evaporator. The solid product was resolved in 15 mL of xylene and then precipitated into n-hexane (200 mL). The crude solid was filtered and then dried. The crude product was purified to column chromatography using chloroform as mobile phase. The target product **HCP-2** was obtained as pure white solid. Yield=40% (0.16 g). Anal. Calc. for $C_{40}H_{26}N_3O_8P_3$ (MW=769.57 g/mol): C, 62.43; H, 3.41; N, 5.46. Found: C, 62.51; H, 3.48; N, 5.49%. FT-IR (KBr, cm^{-1}): 3027 and 3063 $\nu_{C-H(Aromatic)}$, 2923 $\nu_{C-H(Aliphatic)}$, 1736 $\nu_{C=O}$, 1583, 1605 and 1633 $\nu_{C=C}$, 1174 and 1193 $\nu_{P=N}$, 977 ν_{P-O-Ph}. ^{31}P NMR ($CDCl_3$) δ/ppm: 36.60 (2P, t, $P_A(O_2C_{12}H_8)$), 24.65 (1P, *d*, $P_B(O_4C_{16}H_{10})$). ^{1}H NMR ($CDCl_3$) δ/ppm: 2.63 (3H, s, H^{22}), 7.02–7.73 (23H, m, H^3, H^4, H^5, H^6, H^{11}, H^{12}, H^{13}, H^{17}, H^{19}, H^{20} and H^{21}). ^{13}C NMR ($CDCl_3$) δ/ppm: 147.81 C^1, 128.49C^2, 126.51C^3, 129.74C^4, 129.94C^5, 122.03 C^6, 146.93 C^7, 146.93 C^8, 126.06 C^9, 116.40 C^{10}, 122.32 C^{11}, 108.77 C^{12}, 139.91 C^{13}, 138.16 C^{14}, 159.02 C^{15}, 138.74 C^{16}, 125.62 C^{17}, 134.42 C^{18}, 128.65 C^{19}, 130.12 C^{20}, 129.14 C^{21} and 21.96 C^{22}.

2.2.3. Synthesis procedure of 2,2,4,4-bis[spiro(7,8-dioxy-3-(3-methylphenyl)coumarin)]-6,6-bis[spiro(2′,2"-dioxy-1′,1"-biphenylyl)] cyclotriphosphazene (HCP-4)

HCP-3 (0.35 g, 0.76 mmol) and Na_2CO_3 (1.28 g, 12.16 mmol) were dissolved in 50 mL of dry xylene (mixture of isomers) in a 150 mL three-necked reaction flask. 7,8-dihydroxy-3-(3-methylphenyl) coumarin **(1b)** (0.81 g, 3.04 mmol) in 25 mL of xylene was slowly added to the stirred solution at 0 °C. After the reaction mixture was continued for 25 min at 0 °C, it was refluxed in xylene for 48 h. After stopping the reaction, the mixture was filtered to separate the formed sodium chloride. Xylene was evaporated at rotary evaporator. The solid product was resolved in 15 mL of xylene and then precipitated into n-hexane (200 mL). The crude solid was filtered and then dried. The crude product was purified to column chromatography using chloroform as mobile phase. The target product **HCP-4** was obtained as pure white solid. Yield=46% (0.3 g). Anal. Calc. for $C_{44}H_{28}N_3O_{10}P_3$ (MW=851.62 g/mol): C, 62.05; H, 3.31; N, 4.93. Found: C, 62.12; H, 3.38; N, 4.99%. FT-IR (KBr, cm^{-1}): 3060 $\nu_{C-H(Aromatic)}$, 2917 $\nu_{C-H(Aliphatic)}$, 1738 $\nu_{C=O}$, 1585, 1604 and 1633 $\nu_{C=C}$, 1185 and 1210 $\nu_{P=N}$, 948 ν_{P-O-Ph}. ^{31}P NMR ($CDCl_3$) δ/ppm: 35.94 (1P, *d*, $P_A(O_2C_{12}H_8)$), 23.92 (2P, t, $P_B(O_4C_{16}H_{10})$). ^{1}H NMR ($CDCl_3$) δ/ppm: 2.44 (6H, s, H^{22}), 7.02–7.73 (22H, m, H^3, H^4, H^5, H^6, H^{11}, H^{12}, H^{13}, H^{17}, H^{19}, H^{20} and H^{21}). ^{13}C NMR ($CDCl_3$) δ/ppm: 147.51 C^1, 128.34 C^2, 126.81 C^3, 130.91 C^4, 130.02 C^5, 121.90 C^6, 146.64 C^7, 146.57 C^8, 127.19 C^9, 116.77 C^{10}, 122.65 C^{11}, 108.58 C^{12}, 139.71 C^{13}, 138.22 C^{14}, 158.80 C^{15}, 138.96 C^{16}, 125.62 C^{17}, 134.33 C^{18}, 128.46 C^{19}, 129.84 C^{20}, 129.14 C^{21} and 21.53 C^{22}.

2.3. Fabrication of the diodes

Firstly, the native oxide layer on p-Si substrates was removed by etching of HF. The Si substrates were chemically cleaned (methanol, acetone and deionized water baths) for 10–15 min and dried with nitrogen. The solutions of HCP-2 and HCP-4 organic materials and were coated on p-Si having aluminium (Al) ohmic contact by drop coating method. After coating procedure, the films were dried at 50 °C for 10 min. Aluminium metal was evaporated on p-Si wafer to form ohmic contact. After evaporation procedure, the substrates were annealed at 570 °C for 5 min in nitrogen atmosphere. The top electrode of the diode was prepared by Al metal on the films with a diode contact area of 7.85×10^{-3}. The photoresponse properties of the diodes were carried out using FYtronix Electronic Device characterization system (Scheme 1) in dark and illumination conditions. The intensity of solar light is controlled using a FYtronix Electronic Device characterization system.

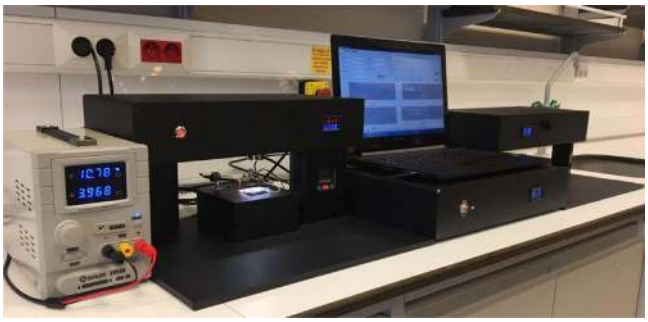

Scheme 1. FYTRONIX Electronic Device characterization system.

3. Results and discussion

3.1. Synthesis

7,8-dihydroxy-3-(3-methylphenyl)coumarin **(1b)** has been obtained at good yield that from the reaction with compound **1a** of pyridinium hydrochloride with using of silica gel as support material by microwave irradiation under solventless conditions. The reactions of **HCP-1** with 1.1 equiv. of 7,8-dihydroxy-3-(3-methylphenyl)coumarin **(1b)** in the presence of Na_2CO_3 in dry xylene (mixture of isomers) gave 2,2-bis[spiro(7,8-dioxy-3-(3-methylphenyl)coumarin)]-4,4,6,6-bis[-spiro(2′,2"-dioxy-1′,1"-biphenylyl)]cyclotriphosphazene **(HCP-2)**. The reactions of **HCP-3** with 2.1 equiv. of **1b** gave 2,2,4,4-bis[-spiro(7,8-dioxy-3-(3-methylphenyl)coumarin)]-6,6-bis[spiro(2′,2"-dioxy-1′,1"-biphenylyl)]cyclotriphosphazene **(HCP-4)**.

The structures of compounds were identified by using elemental analysis, ^{1}H, ^{13}C-APT, ^{31}P (only phosphazene compounds) and 2D HETCOR NMR and FT-IR spectroscopy methods. General presentation of compounds is shown in Scheme 2.

The nitrile peaks (-C≡N) in the structure of **1a** were not observed at FT-IR spectra of **1b**. The -OCH_3 groups in the compound **1a** were converted to the -OH functional groups. The presence of -OH stretching vibration in the FT-IR spectra of **1b** proves that -OCH_3 groups in the compound **1a** and converted to the -OH groups. The OH stretching vibration for **1b** was showed at 3316 and 3477 cm^{-1}. The -C=O stretching vibrations, which are exhibit at 1676 cm^{-1}, is characteristic for coumarin compound. The –OCH_3 protons were not observed at ^{1}H NMR spectrum of **1b.** ^{1}H and ^{13}C NMR spectra of **1b** were showed in Fig. 1. The –OH protons in the structure of **1b** (7 and 8 no. protons in the Scheme 1) were exhibited at 9.44 and 10.17 ppm.

The OH stretching vibrations in the structure of compound **1b** were not observed in the FT-IR and ^{1}H NMR spectra of compounds **HCP-2** and **HCP-4**. The aromatic -CH stretching frequencies at the FT-IR of **HCP-2** and **HCP-4** were showed between 3027 and 3063 cm^{-1}. The carbonyl group in the structures of compounds **HCP-2** and **HCP-4** was showed at 1736 and 1738 cm^{-1}, respectively. The -P=N stretching frequencies, which are observed between 1174 and 1210 cm^{-1}, are characteristic of phosphazene compounds. The P-O-Ph stretching vibration for **HCP-2** and **HCP-4** was exhibited at 977 and 948 cm^{-1}.

The ^{31}P NMR spectra for **HCP-2** and **HCP-4** are showed in Fig. 2 (AB_2 system). There are two peaks in the ^{31}P NMR spectra of dioxyphenylcoumarin substituted **HCP-2** and **HCP-4** compounds. The ^{31}P NMR spectra for **HCP-2** give two sets of peaks around δ=36.60 and 24.65 ppm in a doublet-triplet. At **HCP-4** give two sets of peaks around δ=23.92 and 35.94 ppm in a doublet-triplet.

The characteristic peaks in the ^{1}H and ^{13}C NMR spectra of **HCP-2** and **HCP-4** were given in the Experimental section in detail. The ^{13}C APT NMR spectra of **HCP-2** are given in Fig. 3. The carbonyl carbon

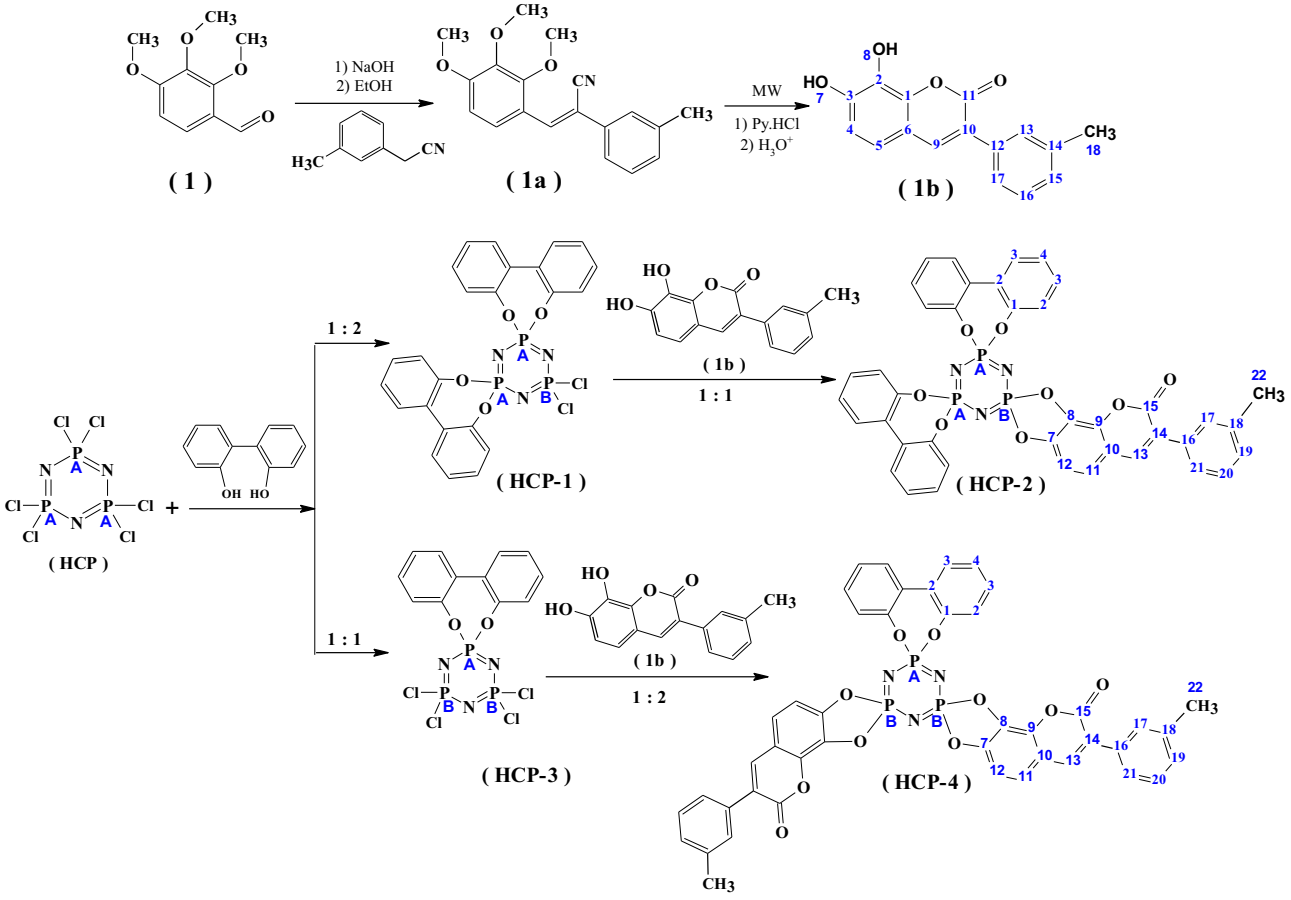

Scheme 2. General synthetic procedures of reactions.

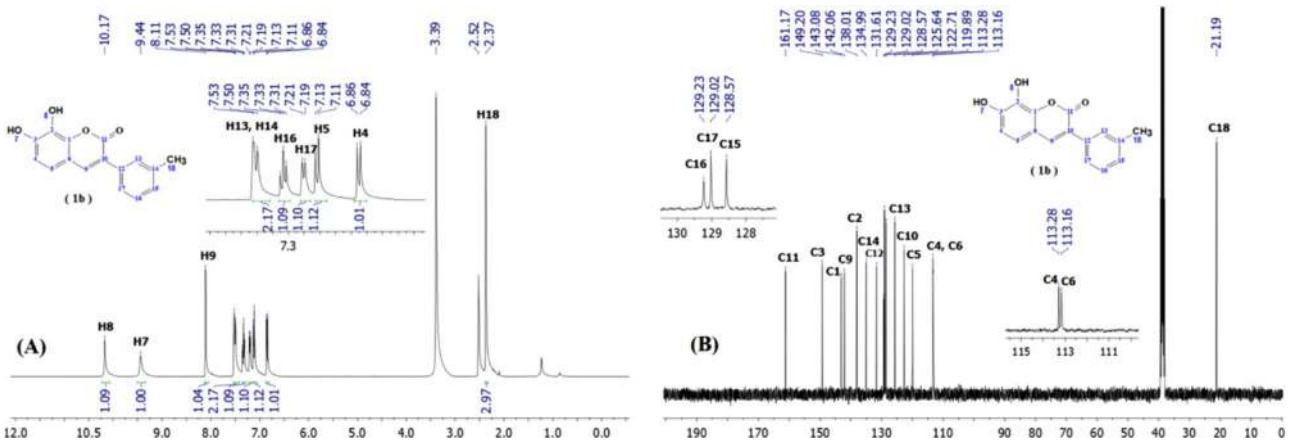

Fig. 1. (A) ^{1}H NMR spectrum and (B) ^{13}C NMR spectrum of **1b** (DMSO-d_6).

peaks (C=O, C^{15}) for **HCP-2** and **HCP-4** was showed at 159.02, 158.80 ppm, respectively. The methyl carbon (-CH_3, C^{22}) for **HCP-2** and **HCP-4** was observed at 21.39 and 21.53 ppm, respectively.

In addition, the ratio of the protons integral height in the ^{1}H NMR spectra supports the proposed structures. In addition, the places of primary, secondary and tertiary carbon atoms were supported with ^{13}C-APT NMR technique.

3.2. I-V characteristics for Al/HCP-2/p-Si/Al and Al/HCP-4/p-Si/Al diodes

The diode characteristics for mono and di substituted dioxyphenylcoumarin bearing cyclotriphosphazene compounds (**HCP-2** and **HCP-4**) are shown in Fig. 4. It is well known that substitution doping process is very important in increasing free charge carriers [20]. As can be seen, the Al/HCP-2/p-Si/Al diode of high rectification behaviour with rectification ratio *RR* of 2.15×10^6 at 3 V. Schottky diode parameters such as ideality factor *n* and barrier height ϕ_b were calculated from (I-V) characteristics curve in dark and at room temperature by using the thermionic emission theory [21–23]:

$$I = I_o \exp\left(\frac{q(V - IR)}{nkT}\right)\left[1 - \exp\left(-\frac{q(V - IR_s)}{kT}\right)\right] \quad (1)$$

where I is the current through a Schottky diode, V is the applied voltage, q is the electronic charge, k is the Boltzmann constant, T is the absolute temperature, R_s is the series resistance, *n* is the ideality factor can be calculated by using the following equation [24,25]:

$$n = \frac{q}{kT}\frac{dV}{d\ln(I)}, \quad \text{and}$$

I_o is the saturation current given by [26,27]:

$$I_o = AA^*T^2 \exp\left(\frac{-q\phi_b}{kT}\right) \quad (2)$$

where, A^* is the effective Richardson's constant equal (32 A cm^{-2} k^{-2} for p-type silicon), A is the effective diode area and ϕ_b is the zero bias effective barrier height is expressed by the following relation [28]:

$$\phi_b = (kT/q)\ln(AA^*T^2/I_o) \quad (3)$$

According to Fig. 4 it can be observed that the forward current I_f of **HCP-2** compound with greater value compared with **HCP-4** compound this behaviour is believed to be due to mono substituted dioxyphenylcoumarin of high chemical molecular interaction and high electron density [29,30]. The diode parameters of Al/HCP-2/p-Si/Al and Al/HCP-4/p-Si/Al devices have been estimated and presented in Table 1. Al/HCP-2/p-Si/Al shows very small saturation current I_o compared to Al/HCP-4/p-Si/Al. It is also evaluated that the ideality factor n with values greater than unity attributed by the presence of deep levels and interfacial states between organic material and semiconductor. In order to determine the values of series resistance R_s and shunt resistance R_{sh} of the photodiode in dark and at room temperature we can use the equation [31]:

$$R_j = \frac{\partial V}{\partial I} \quad (4)$$

where, R_j is the junction resistance of the diode. Fig. 5 shows (R_j-V) plots for Al/HCP-2/p-Si/Al and Al/HCP-4/p-Si/Al diodes. R_s and R_{sh} for the synthesized diodes were calculated and tabulated in Table 1. It is noted from Fig. 5 that, the Al/HCP-2/p-Si/Al diode of low series resistance and high shunt resistance which indicates that the diode of

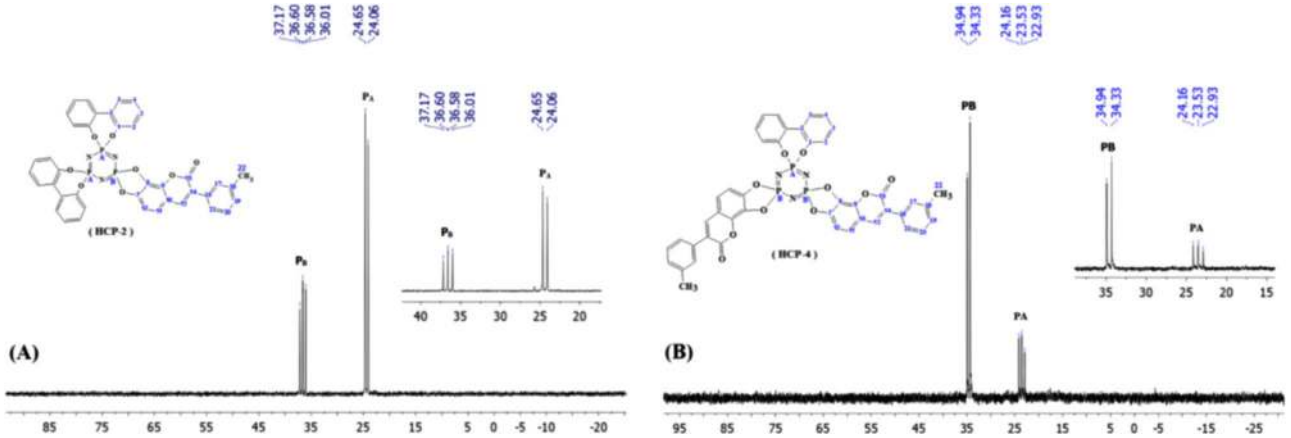

Fig. 2. (A) ^{31}P NMR spectrum of **HCP-2** and (B) ^{31}P NMR spectrum of **HCP-4** (in $CDCl_3$).

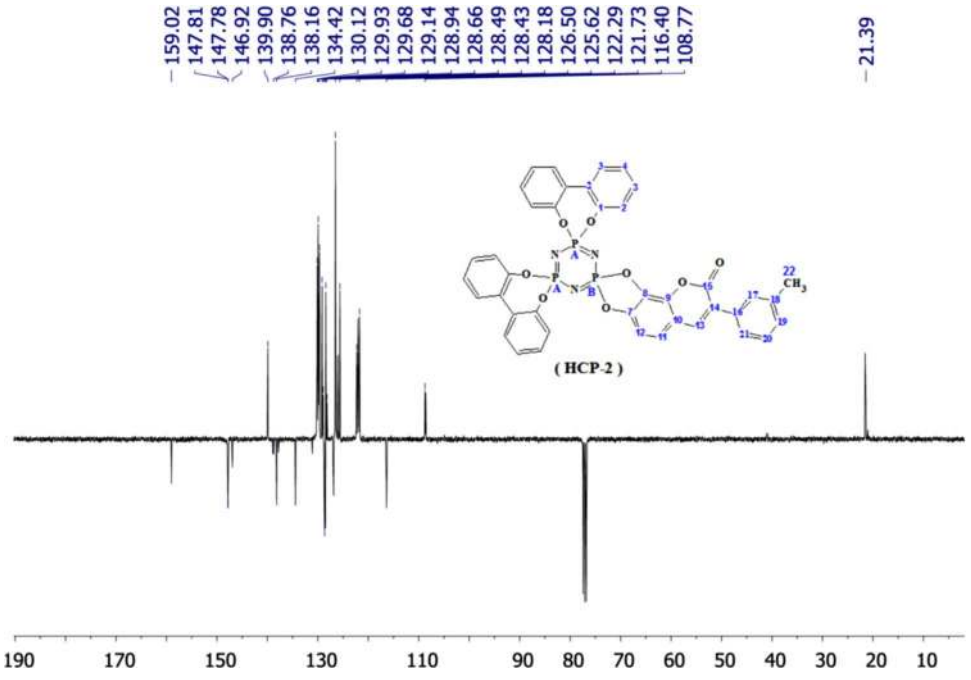

Fig. 3. ^{13}C APT NMR spectrum of **HCP-2** (in $CDCl_3$).

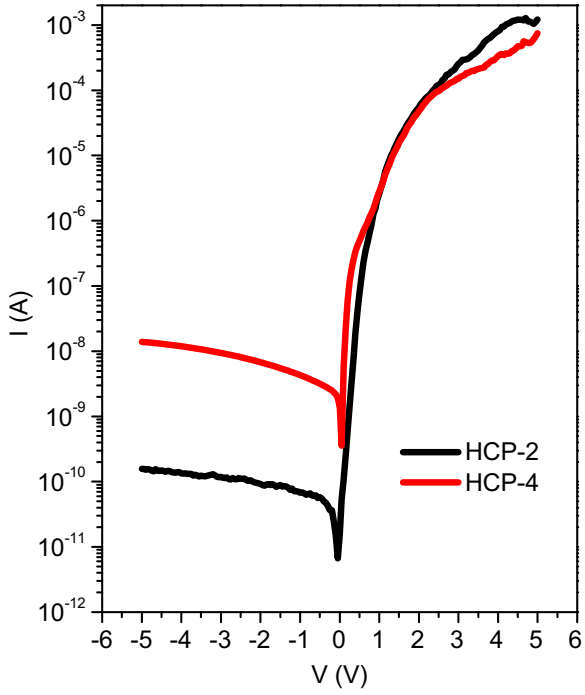

Fig. 4. *I* – V Characteristics of Al/HCP-2/p-Si/Al and Al/HCP-4/p-Si/Al diodes in dark and at room temperature.

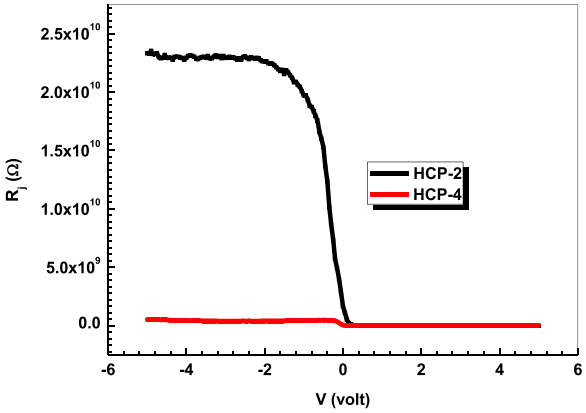

Fig. 5. Plot of $R_j$vs. V for Al/HCP-2/p-Si/Al and Al/HCP-4/p-Si/Al diodes in dark and at room temperature.

mono substituent dioxyphenylcoumarin bearing cyclotriphosphazene compound is mostly favoured by larger electron rich substituent and this is related to the arrangement of dioxyphenylcoumarin groups [30–32].

On the other hand, the barrier height $\phi_b$and series resistance $R_s$of the photodiode can be determined by other theory known as Nord's method introduced by the equation [33]:

$$F(V) = \frac{V}{\gamma} - \frac{kT}{q} \ln\left(\frac{I(V)}{AA^{*}T^{2}}\right) \quad (5)$$

where, γ is the first integer greater than ideality factor n. I(V) is the

Table 1
Schottky parameters for Al/HCP-2/p-Si/Al and Al/HCP-4/p-Si/Al diode obtained from (I – V) characteristics, Nord's equation and (C – V) plots.

photodiode	(I-V) Characteristics						Nord's model		(C-V) Measurements
	n	ϕ_b(eV)	R_s(Ω)	$I_o\times10^{-10}$	$RR\times10^4$	$R_{sh}\times10^8$(Ω)	$R_s\times10^5$(Ω)	ϕ_b(eV)	ϕ_b(eV)
Al/HCP–2/p-Si /Al	2.29	0.87	2960	0.2	215	330	2.3	0.97	0.24
Al/HCP–4/p-Si /Al	1.71	0.79	8883	5	1.6	3.8	3.47	0.82	0.25

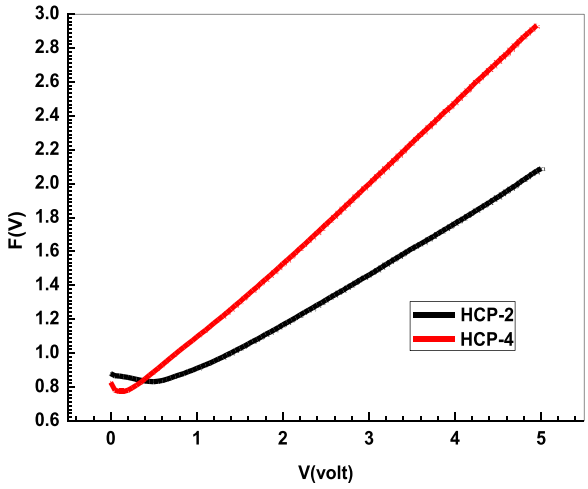

Fig. 6. F(V) versus V plots for Al/HCP-2/p-Si/Al and Al/HCP-4/p-Si/Al diodes in dark and at room temperature.

current obtained from the I–V characteristics. The barrier height ϕ_b of the prepared diode can be obtained from equation [34]:

$$\phi_b = F(V_o) + \frac{V_o}{\gamma} - \frac{kT}{q} \quad (6)$$

where $F(V_o)$ the minimum point of F(V) demonstrated in Fig. 6 and $V_o$is the corresponding voltage. The series resistance of the junctions can be calculated as follows [35]:

$$R_s = \frac{kT(\gamma - n)}{qI(V_o)} \quad (7)$$

where I is the corresponding current. ϕ_b and R_s of the synthesized diodes were determined and listed in Table 1. It worth to note that, the Al/HCP-2/p-Si/Al diode of low series resistance compared to other one which is consistent with the results obtained from I-V characteristics.

3.3. Photoresponse properties of Al/HCP-2/p-Si/Al and Al/HCP-4/p-Si/Al diodes

The study of photoconductivity for both mono and di substituted dioxyphenylcoumarin bearing cyclotriphosphazene compounds (**HCP-2** and **HCP-4**) under different power intensity plays a key role in optoelectronic applications [36]. It is seen in Fig. 7(a and b) that, the prepared diodes with high photocurrent response and Al/HCP-2/p-Si/Al diode with high photoconductivity and more of free carriers affected by incident light [37].

Fig. 8(a and b) shows the influence of light intensity on the prepared device conductivity. It can be seen that the current of the photodiode increase through incident of light and remain constant until turning off light reach its initial value. This is dependent on the presence of charge carriers trapped in localized states within band gap [38]. The trapped charge carriers overcome the optical gap by increasing illumination power intensity suggests that these states have significant influence on the transport mechanism [39].

It is observed from this behaviour that power intensity activate the transport of charge carriers [40]. The photodiode conductivity affected by trap centers response to the influence of various illuminations intensities this can be described according to the following relation [41]:

$$I_{Ph} = AP^m \quad (8)$$

where I_{Ph} is the photocurrent, A is a constant, P is the illumination intensity and m is an exponent. According to Fig. 9, the exponent m for Al/HCP-2/p-Si/Al and Al/HCP-4/p-Si/Al diodes were determined from the slope with values 0.6 and 1.34 respectively. The values of

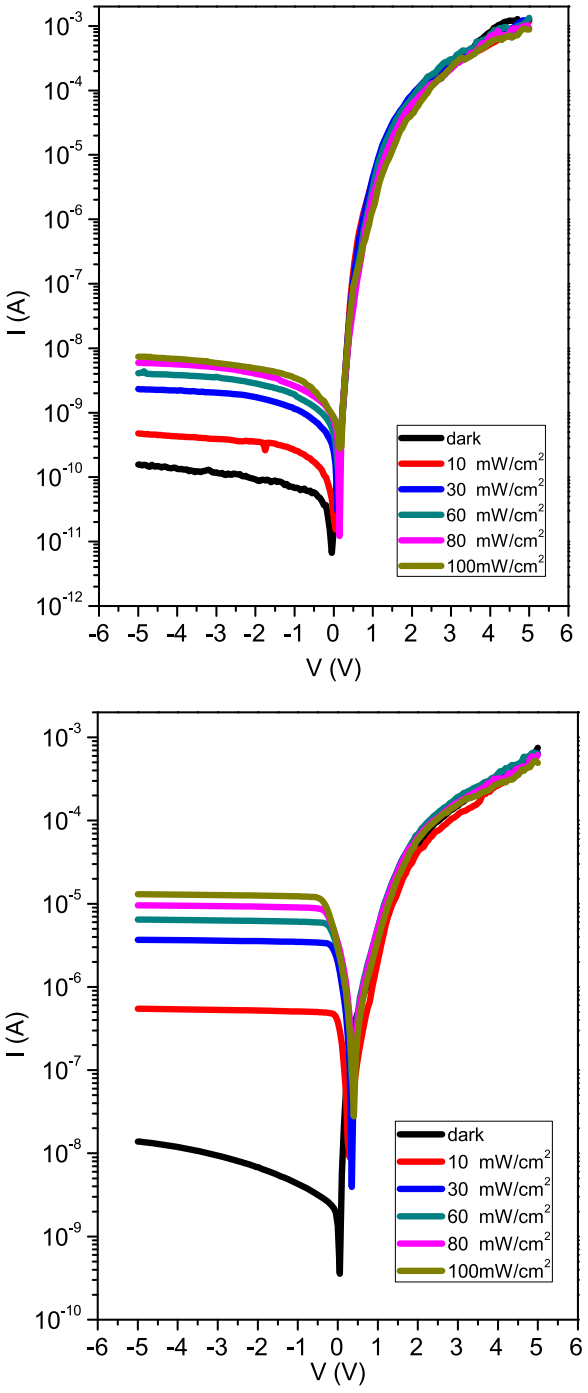

Fig. 7. (a and b). *I* – V plots **(a)** Al/HCP-2/p-Si/Al and **(b)** Al/HCP-2/p-Si/Al diodes under various light intensities.

exponent m enhance the presence of trap centers within optical band gap which increase the photodiode conductivity [42].

3.4. (**C–V**), (**G–V**)*and* (**Rs–V**) *characteristics of the prepared photodiodes*

Fig. 10 (a and b) shows the influence of applied frequency varies from 10 kHz to 1 MHz on capacitance-voltage (C – V) and corrected capacitance-voltage (C_{adj}–V) of Al/HCP-2/p-Si/Al diode. It can be seen from Fig. 10 (a) that the capacitance is constant in forward region and decrease with increasing frequency in the reverse bias voltages [43]. Moreover, a peak appears at nearly −3.5 V and shifts to higher voltage with applied frequency. This behaviour can be explained by the change in transport of electric charge in depletion region or may be due to

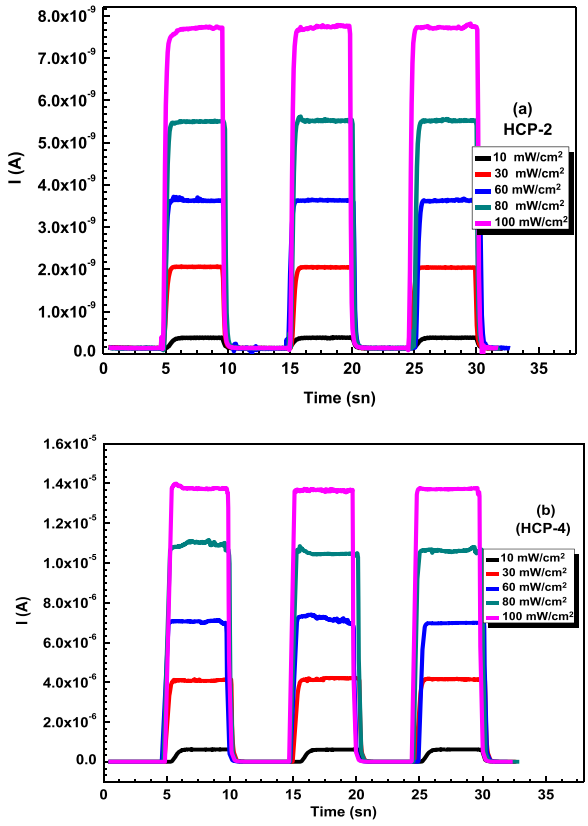

Fig. 8. (a and b). Phototransient current plots of (a) Al/HCP-2/p-Si/Al and (b) Al/HCP-4/p-Si/Al photodiodes.

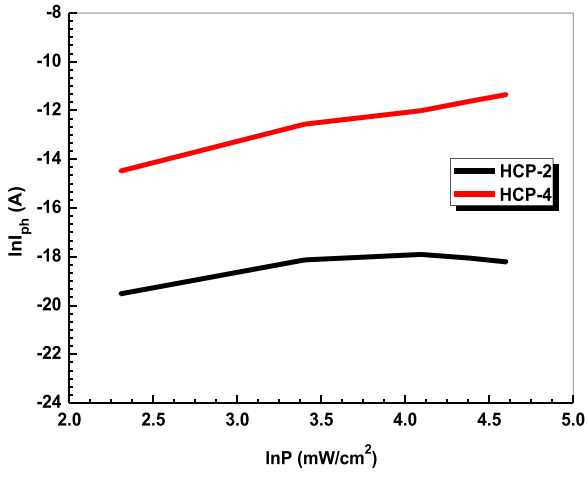

Fig. 9. $\ln I_{ph}$ versus $\ln_p$ of Al/HCP-2/p-Si/Al and Al/HCP-4/p-Si/Al diodes.

recombination process influenced by applied alternating current voltage [44]. Fig. 10 (b) indicates the (C_{adj}–V) plots for Al/HCP-2/p-Si/Al diode. The capacitance of the photodiode affected by series resistance so it can be corrected by using the following equations [45,46]:

$$C_{adj} = \frac{[G_m^2 + (\omega \quad C_m)^2]C_m}{a^2 + (\omega \quad C_m)^2} \tag{9}$$

$$a = \quad G_m - \quad [G_m^2 + (\omega \quad C_m)^2]R_s \tag{10}$$

where C_{adj} is the corrected capacitance, R_s is the series resistance, $\omega = 2\pi f$ is the angular frequency and C_m and G_m are the measured capacitance and conductance respectively [47]. It is noted that the corrected capacitance remains constant in forward region. In addition,

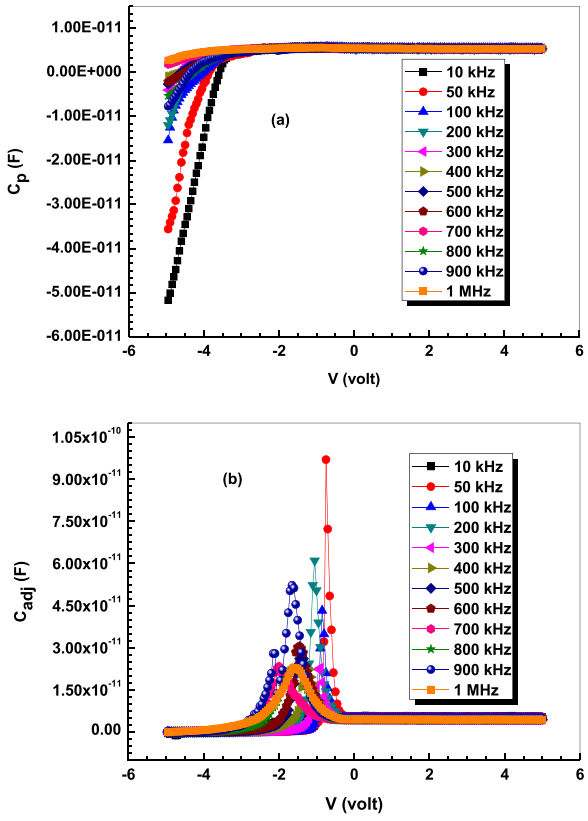

Fig. 10. (a and b). (a) C – V and (b) C_{adj}–V characteristics for Al/HCP-2/p-Si/Al diode.

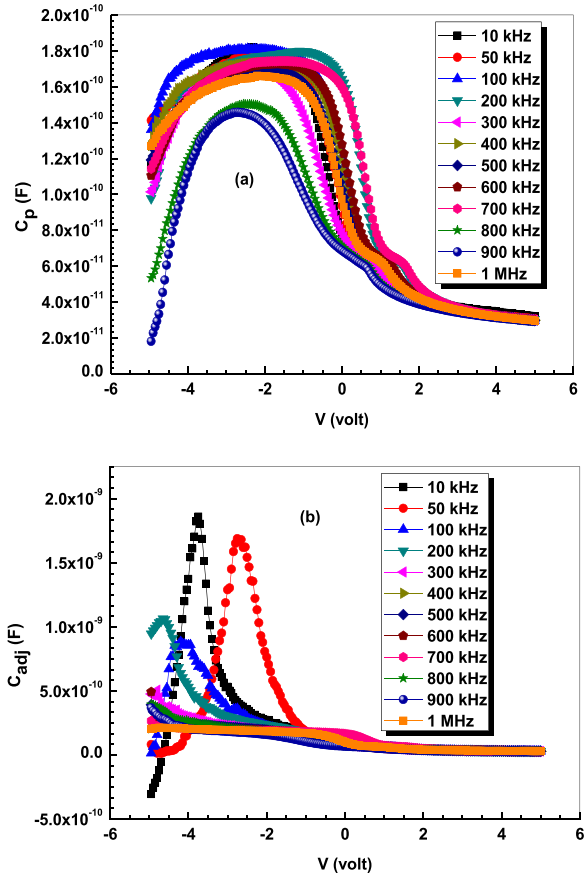

Fig. 11. (a and b). (a) C – V and (b) C_{adj}–V characteristics for Al/HCP-4/p-Si/Al.

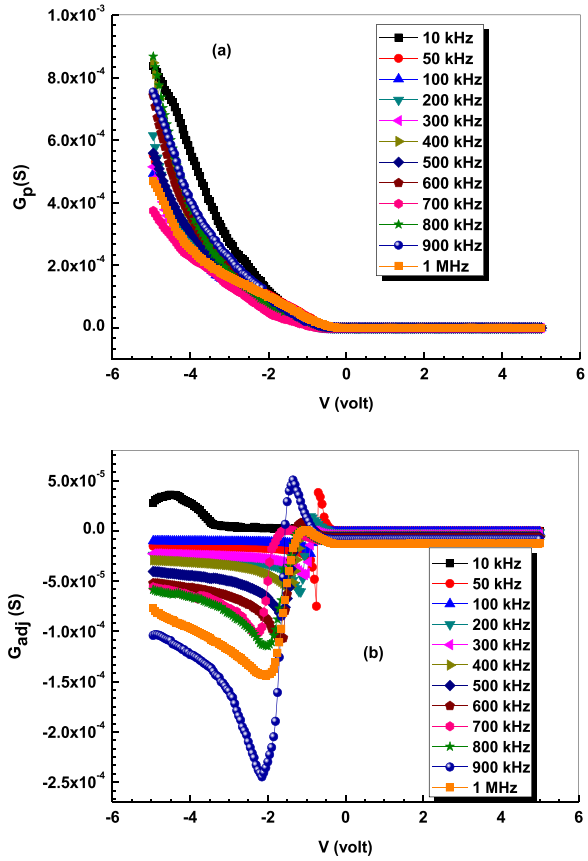

Fig. 12. (a and b). (a) G − Vand (b) G_{adj}−Vcharacteristics for Al/HCP-2/p-Si/Al diode.

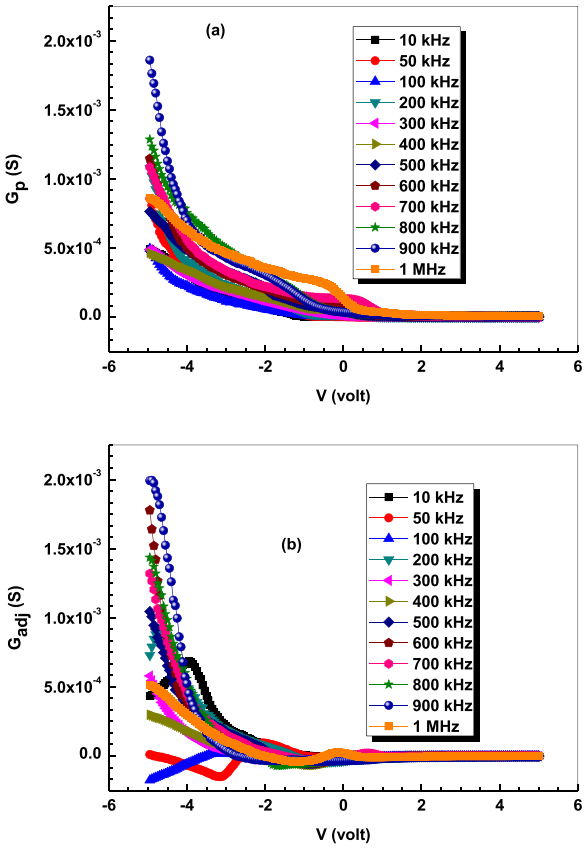

Fig. 13. (a and b). (a) G − Vand (b) G_{adj}−Vcharacteristics for Al/HCP-4/p-Si/Al diode.

there is a peak appears at −1.5 V in the reverse bias shifts irregularly to higher voltage [48].

Fig. 11 (a and b) demonstrates the variation of capacitance-voltage (C − V) and corrected capacitance-voltage (C_{adj}−V) of Al/HCP-4/p-Si/Al diode with applied different frequencies [49]. It is noteworthy that (C − V) and (C_{adj}−V) varies independent of applied frequency may be due to the change of the geometric and dielectric properties of the photodiodes [50,51].

The conductance-voltage (G − V) and corrected conductance-voltage (G_{adj}−V) for Al/HCP-2/p-Si/Al diode have been measured as a function of frequency and are given in Fig. 12 (a and b). According to Fig. 12 (a), the conductance changes with applied frequency. It is observed that the conductance become constant in forward bias and starts to increase at −0.35 V in the reverse bias [52]. On other hand, the conductance of the photodiode is affected by series resistance can be expressed using the following equation [53]:

$$G_{adj} = \frac{[G_m^2 + (\omega \quad C_m)^2]a}{a^2 + (\omega \quad C_m)^2} \tag{11}$$

where G_{adj} is the corrected conductance. Fig. 12 (b) shows the variation of corrected conductance-voltage (G_{adj}−V) independence of applied various frequencies which confirms the effect of series resistance and change of charge carriers distribution in the depletion region with applied various frequencies [54].

Fig. 13 (a and b) demonstrate the change of conductance-voltage (G − V) and corrected conductance-voltage (G_{adj}−V) of Al/HCP-4/p-Si/Al diode with applied frequency [55]. It can be seen that both of (G − V) and (G_{adj}−V) varies with applied frequency in the reverse bias voltage and become constant in the forward bias voltage [55].

The series resistance R_s of the prepared diodes can be determined from measured capacitance and measured conductance using the following equation [56]:

$$R_s = \frac{G_m}{G_m^2(\omega C_m)^2} \tag{12}$$

where, C_m and $G_m$are the measured capacitance and conductance, respectively. Fig. 14 (a and b) demonstrates the variation of series resistance-voltage (R_s−V) with applied different frequencies for Al/HCP-2/p-Si/Al and Al/HCP-4/p-Si/Al diodes respectively. It can be seen that the series resistance of the two devices decrease with applied frequency [57]. Fig. 14 (a), shows a peak appears at −0.35 V in reverse bias and shifts to higher voltage. The broadening of the peak increase with frequency suggests the influence of interface states to applied frequency and the increase of charge carriers [58]. On other side, Fig. 14 (b), indicates two peaks appears at −1.15 V and −0.15 V in reverse bias and shift to positive voltage with increasing frequency [59].

The capacitance of a Schottky barrier diode can be determined from the equation [60]:

$$\frac{1}{C^2} = \frac{2(V_{bi}+V)}{q\varepsilon_s\varepsilon_o A^2 N_a} \tag{13}$$

where N_a is the doping concentration, V_{bi} the built-in voltage, V the applied voltage and ε_s is the static dielectric constant and ε_o=8. 85 × 10^{-14} F/cm. Fig. 15 (a and b) shows the ($1/C^2$−V) plot measured at 1 MHz frequency for Al/HCP-2/p-Si/Al and Al/HCP-4/p-Si/Al diode respectively. The built-in voltage has been calculated from an extrapolation of the linear ($1/C^2$−V)to the V − axis and N_a is estimated from the slope of ($1/C^2$−V) curve [61]. The barrier height ϕ_b of the synthesized diodes can be investigated from the following relation [62]:

$$\phi_b = V_{bi} + \frac{kT}{q}\left[1 + \ln\frac{N_v}{N_a}\right] \tag{14}$$

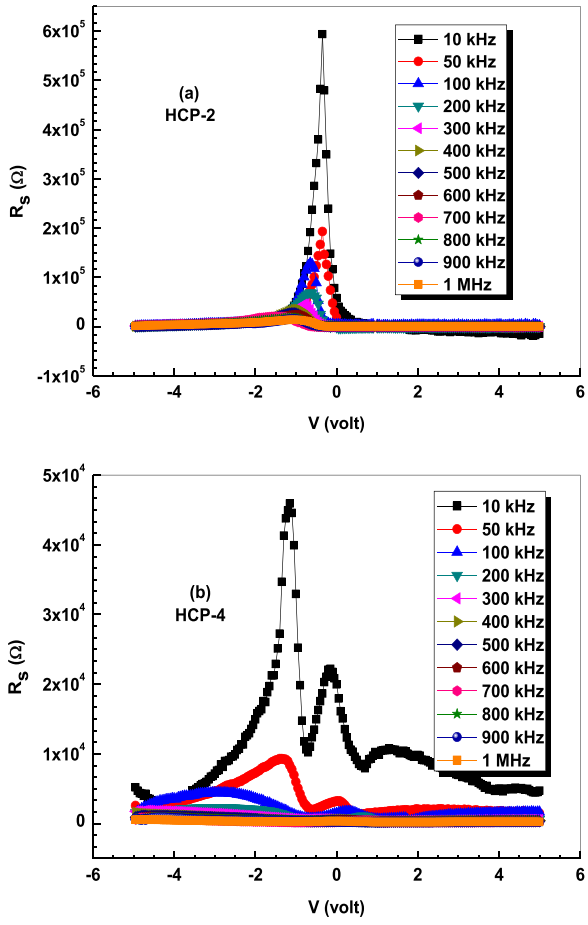

Fig. 14. (a and b). (R_s–V)characteristics for (a) Al/HCP-2/p-Si/Al and (b) Al/HCP-4/p-Si/Al diodes.

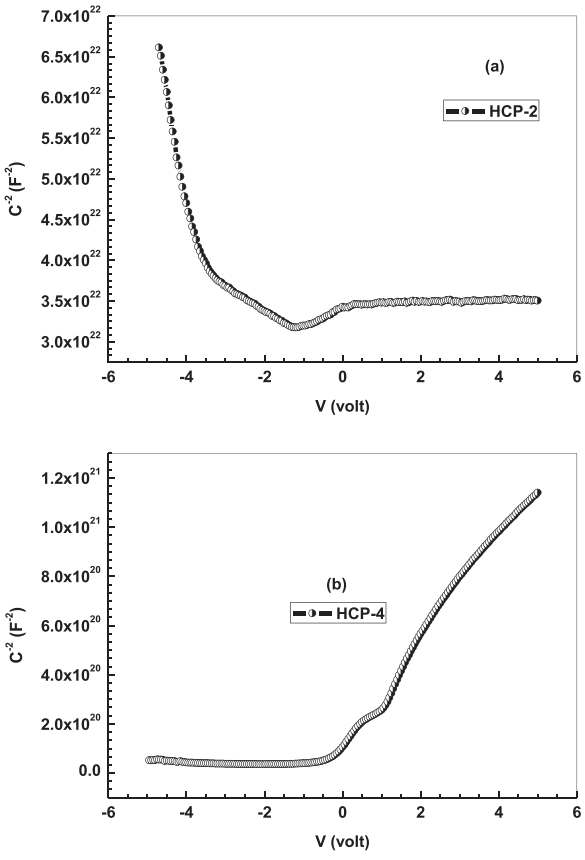

Fig. 15. (a and b). (C^{-2}–V) for (a) Al/HCP-2/p-Si/Al and (b) Al/HCP-4/p-Si/Al diodes.

where N_v (N_v=182×10^{19} cm^{-3}) is the density of states in the valence band of silicon [63]. The values of barrier height of Al/HCP-2/p-Si/Al and Al/HCP-4/p-Si/Al diodes have been estimated from (C – V)measurements and are listed in Table 1. The results indicate that there are high differences in the values of barrier height obtained from I-V and C-V calculations [64]. This can be explained by the change of energy level at interface states or the change of trapped charges due to the existence of deep levels and localized states at the interfaces of organic-semiconductor contact [65].

4. Conclusions

Mono and di substituted dioxyphenylcoumarin bearing cyclotriphosphazene compounds (**HCP-2** and **HCP-4**) were prepared from the reaction of **HCP-1** and **HCP-3** with compound **1b**, respectively. The photodiode characteristics of Al/HCP-2/p-Si/Al and Al/HCP-4/p-Si/Al devices were investigated from I – V and C – V measurements. Electrical properties of the synthesized diodes and Schottky parameters such as ideality factor n, series resistance R_s and barrier height ϕ_b have been determined in dark and at room temperature from I-V characteristic curve and Norde's equation. The Al/HCP-2/p-Si/Al diode indicates a high rectification ratio and high shunt resistance. The photoresponse properties of the diodes indicate that the photodiodes exhibited a high photocurrent response. It is evaluated that the fabricated diodes can be used a photosensor for solar tracking systems.

Acknowledgements

The authors are grateful to the Research Fund of the TUBITAK for their support (for the synthesis of compounds) with the project No-110T652 and the photochemical applications supported by the Firat University Research Fund (Project no: FF.16.19). Also, authors would like to acknowledge the support of the King Khalid University for this research through a grant RCAMS/KKU/002-16 under the (Research Center for Advanced Materials Science) at King Khalid University, Kingdom of Saudi Arabia.

References

[1] H.R. Allcock, Phosphorus-Nitrogen Compounds: Cyclic, Linear and Polymeric Systems, Academic Press Inc, New York, 1972.
[2] Y. Tumer, N. Asmafiliz, Z. Kılıc, T. Hokelek, L.Y. Koc, L. Acık, M.L. Yola, A.O. Solak, Y. Oner, D. Dundar, M. Yavuz, Phosphorus–nitrogen compounds: part 28. Syntheses, structural characterizations, antimicrobial and cytotoxic activities, and DNA interactions of new phosphazenes bearing vanillinato and pendant ferrocenyl groups, J. Mol. Struct. 1049 (2013) 112–114.
[3] E.T. McBee, K. Okuhara, C.J. Morton, Modified Friedel-Craf ts Preparation of 2,2,4,4-Tetrachloro-6,6-diphenylcyclotriphosphazatrie, Inorg. Chem. 4 (1965) 1672–1673.
[4] M. Reynes, D. Virieux, O. Jeannin, M. Fourmigue, J. Moreau, O.J. Dautel, Crystal structure of tris(binol)cyclotriphosphazene. A new clathration system, Tetrahedron Lett. 57 (2016) 4086–4089.
[5] K. Koran, F. Özen, G. Torğut, G. Pıhtılı, E. Çil, A.O. Görgülü, M. Arslan, Synthesis, characterization and dielectric properties of phosphazenes containing chalcones, Polyhedron 78 (2014) 213–220.
[6] E. Şenkuytu, E.T. Eçik, M. Durmuş, G.Y. Çiftçi, Monofunctional amines substituted fluorenylidene bridged cyclotriphosphazenes: 'turn-off' fluorescence chemosensors for Cu^{2+} and Fe^{3+} ions, Polyhedron 101 (2015) 223–229.
[7] H.J. Bolink, E. Barea, R.D. Costa, E. Coronado, S. Sudhakar, C. Zhen, A. Sellinger, Efficient blue emitting organic light emitting diodes based on fluorescent solution processable cyclic phosphazenes, Org. Electron. 9 (2008) 155–163.
[8] M. Sezgin, O. Ozay, S. Koyuncu, H. Ozay, F.B. Koyuncu, A neutral state colorless phosphazene/carbazole hybride dendron ond its electrochromic device application, Chem. Eng. J. 274 (2015) 282–289.
[9] L. Xia, Y. Xia, Z. Liu, A novel fluorocyclophosphazene as bifunctional additive for safer lithium-ion batteries, J. Power Sources 278 (2015) 190–196.
[10] Y.J. Shin, Y.R. Ham, S.H. Kim, D.H. Lee, S.B. Kim, C.S. Park, Y.M. Yoo, J.G. Kim, S.H. Kwon, J.S. Shin, Application of cyclophosphazene derivatives as flame retardants for ABS, J. Ind. Eng. Chem. 16 (2010) 364–367.

[11] A.O. Görgülü, K. Koran, F. Ozen, S. Tekin, S. Sandal, Synthesis, structural characterization and anti-carcinogenic activity of new cyclotriphosphazenes containing dioxybiphenyl and chalcone groups, J. Mol. Struct. 1087 (2015) 1–10.
[12] E. Okutan, B. Çoşut, S.B. Kayıran, M. Durmuş, A. Kılıç, S. Yeşilot, Synthesis of a dendrimeric phenoxy-substituted cyclotetraphosphazene and its non-covalent interactions with multiwalled carbon nanotubes, Polyhedron 67 (2014) 344–350.
[13] K.P.K. Naik, V. Sreeramulu, E. Ramya, K. Muralidharan, D.N. Rao, Design and synthesis of hyperstructured molecules based on cyclophosphazene core for multiphoton absorption, Med. Chem. Phys. 180 (2016) 38–45.
[14] M.R. Rao, A. Ghosh, M. Ravikanth, Synthesis, spectral and electrochemical properties of cyclotriphosphazene appended with six metalloporphyrins, Inorg. Chim. Acta 372 (2011) 436–441.
[15] F. Özen, S. Tekin, K. Koran, S. Sandal, A.O. Görgülü, Synthesis, structural characterization, and in vitro anti-cancer activities of new phenylacrylonitrile derivatives, Appl. Biol. Chem. 59 (2016) 239–248.
[16] N.P. Buu-Hoi, G. Saint-Ruf, B. Lobert, Oxygen Heterocycles. Part XIV. Hydroxylated 3-Aryl- and 3-Pyridyl-coumarins, J. Chem. Soc. (C) (1969) 2069–2070.
[17] Ş.N.K. Elmas, F. Özen, K. Koran, İ. Yilmaz, A.O. Görgülü, S. Erdemir, Coumarin based highly selective "off-on-off" type novel fluorescent sensor for Cu^{+2} and S^{-2} in aqueous solution, J. Fluoresc. 1 (2016) 1–9.
[18] G.A. Carriedo, L.F. Catuxo, F.J.G. Alonso, P.G. Elipe, P.A. González, Preparation of a new type of phosphazene high polymers containing 2,2'-dioxybiphenyl groups, Macromolecules 29 (1996) 5320–5325.
[19] K. Koran, F. Özen, F. Biryan, A.O. Görgülü, Synthesis, structural characterization and dielectric behavior of new oxime-cyclotriphosphazene derivatives, J. Mol. Struct. 1105 (2016) 135–141.
[20] A.S. Dahlan, A. Tataroğlu, A.A. Al-Ghamdi, A.A. Al-Ghamdi, S. Bin-Omran, Al-Turkı, F. El-Tantaway, F. Yakuphanoglu, Photodiode and photocapacitor properties of Au/CdTe/p-Si/Al device, J. Alloy. Compd. 646 (2015) 1151–1156.
[21] M.M. El-Nahass, H.S. Metwally, H.E.A. El-Sayed, A.M. Hassanien, Electrical and photovoltaic properties of FeTPPCl/p-Si heterojunction, Synth. Met. 161 (2011) 2253–2258.
[22] I. Orak, K. Ejderha, A. Turut, The electrical characterizations and illumination response of Co/N-type GaP junction device, Curr. Appl. Phys. 15 (2015) 1054–1061.
[23] B. Roul, S. Mukundan, G. Chandan, L. Mohan, S.B. Krupanidhi, Barrier height inhomogeneity in electrical transport characteristics of InGaN/GaN heterostructure interfaces, AIP Adv. 5 (2015) 037130.
[24] N.P. Maity, R. Maity, R.K. Thapa, S. Baishya, Image force effect on tunnelling current for ultrathin High-K dielectric material Al_2O_3 based metal oxide semiconductor devices, J. Nanoelectron. Optoelectron. 10 (2015) 645–648.
[25] M.A. Mayimele, J.P.J. van Rensburg, F.D. Auret, M. Diale, Analysis of Temperature dependant current voltage characteristics and extraction of series resistance in Pd/ZnO Schottky barrier diodes, Phys. B: Condens. Matter 480 (2016) 58–62.
[26] J. Lee, T. Uhrmann, T. Dimopoulos, H. Bruckl, J. Fidler, TEM study on diffusion process of NiFe Schottky and MgO/NiFe tunneling diodes for spin injection in silicon, IEEE Trans. Magn. 46 (2010) 2067–2069.
[27] A. Sadakata, K. Osada, D. Taguchi, T. Yamamoto, M. Fukuzawa, T. Manaka, M. Iwamoto, Probing interfacial charge accumulation in ITO/a-NPD/Alq3/Al diodes under two electroluminescence operational modes by electric-field induced optical second-harmonic generation, J. Appl. Phys. 112 (2012) 083723.
[28] H.C. Card, E.H. Rhoderick, Studies of tunnel MOS diodes I. Interface effects in silicon Schottky diodies, J. Phys. D: Appl. Phys. 4 (1971) 1589.
[29] T. Tunç, Ş. Altındal, İ. Dökme, H. Uslu, Anomalous peak in the forward-bias C-V plot and temperature-dependent behaviour of Au/PVA (Ni,Zn-doped) / n-Si(ıı) structures, J. Electron. Mater. 40 (2011) 157–164.
[30] M.F. Bobrov, G.V. Popova, V.G. Tsirel'son, Mono- and diphenoxy-substituted cyclotriphosphazenes: the molecular structure and interatomic interactions, Russ. J. Phys. Chem. A 82 (2008) 1295–1302.
[31] S. Sze, Physics of Semiconductor Devices, Wiley, New York, 1979.
[32] K.S. Karimov, M.M. Ahmed, S.A. Moiz, M.I. Fedorov, Temperature-dependent properties of organic-on-inorganic Ag/p-CuPc/*n*-GaAs/Ag photoelectric cell, Sol. Energ. Mater. Sol. Cells 87 (2005) 61–75.
[33] M.A. Ebeoğlu, F. Temurtas, Z.Z. Özturk, Ag/*n*-GaAs Schottky mis diodes with surface insulating layers prepared using $(NH_4)_2S$ solutions without water, Solid-State Electron. 42 (1998) 23–27.
[34] F. Yakuphanoglu, Y. Caglar, M. Caglar, S. Ilican, ZnO/p-Si heterojuntion photodiode by sol-gel deposition of nanostructure *n*-ZnO film on p-Si substrate, Mater. Sci. Semicond. Process. 13 (2010) 137–140.
[35] H. Norde, A modified forward *I-V* plot for Schottky diodes with high series resistance, J. Appl. Phys. 50 (1979) 5052.
[36] R.F. Bader, Atoms in Molecules: A Quantum Theory, vol. 22 of International Series of Monographs on Chemistry, Clarendon, Oxford, U.K, 1990 (Mir, Moscow, 2001).
[37] F.W. Biegler-Konig, R.F.W. Bader, T.-H. Tang, Calculation of the average properties of atoms in molecules, J. Comput. Chem. 3 (1982) 317–328.
[38] N.M. Khusayfan, A.A. Al-Ghamdi, F. Yakuphanoglu, J. Alloy. Compd. 663 (2016) 796–807.
[39] A.D. Schricker, F.M. Davidson, R.J. Wiacek, B.A. Korgel, Space charge limited currents and trap concentrations in GaAs nanowires, Nanotechnology 17 (2006) 2681–2688.
[40] B.S. Simpkins, M.A. Mastro, C.R. Eddy, J.K. Hite, P.E. Pehrsson, Space-charge-limited currents and trap characterization in coaxial AlGaN/GaN nanowires, J. Appl. Phys. 110 (2011) 044303–044304.
[41] W. Xu, A. Chin, L. Ye, C.Z. Ning, H. Yu, Charge transport and trap characterization in individual GaSb nanowires, J. Appl. Phys. 111 (2012) 104515.
[42] D. Ko, X.W. Zhao, K.M. Reddy, O.D. Restrepo, R. Mishra, T.R. Lemberger, I.S. Beloborodov, N. Trivedi, N.P. Padture, W. Windl, F.Y. Yang, E. Johnston-Halperin, Defect states and disorder in charge transport in semiconductor nanowires, J. Appl. Phys. 114 (2013) 043711.
[43] S. Aksoy, Y. Caglar, Effect of ambient temperature on electrical properties of nanostructure *n*-ZnO/p-Si heterojunction diode, Superlattices Microstruct. 51 (2012) 613–625.
[44] S. Altındal, H. Kanbur, D.E. Yıldız, M. Parlak, Current conduction mechanismin Al/p-Si Schottky barrier diodes with native insulator layer at low temperatures, Appl. Surf. Sci. 253 (2007) 5056–5061.
[45] M.E. Aydin, F. Yakuphanoglu, J.H. Eom, D.H. Hwang, Electrical characterization of Al/MEH-PPV/p-Si Schottky diode by current–voltage and capacitance–voltage methods, Phys. B: Condens. Matter 387 (2007) 239–244.
[46] S.M. Sze, Physics Semiconductor Devices, second ed., NewYork, 1981.
[47] R.T. Tung, Recent advances in Schottky barrier concepts, Mater. Sci. Eng.: R: Rep. 35 (2001) 1–3.
[48] W. Monch, Valence-band offsets and Schottky barrier heights of layered semiconductors explained by interface-induced gap states, Appl. Phys. Lett. 72 (1998) 1899.
[49] E.H. Nicollian, A. Goetzberger, The Si-SiO2 interface-electrical properties as determined by the metal-insulator-silicon conductance technique, Bell Syst. Tech. J. 46 (1967) 1055–1133.
[50] S.K. Sharma, D. Pavithra, G. Sivakumar, N. Srinivasamurthy, B.L. Agrawal, Determination of solar cell diffusion capacitance and its dependence on temperature and 1 MeV electron fluence level, Sol. Energy Mater. Sol. Cells 26 (1992) 169–179.
[51] S.M. Sze, Physics Semiconductor Devices, second ed., New York, 1981.
[52] S.K. Sharma, D. Pavithra, G. Sivakumar, N. Srinivasamurthy, B.L. Agrawal, Determination of solar cell diffusion capacitance and its dependence on temperature and 1 MeV electron fluence level, Sol. Energy Mater. Sol. Cells 26 (1992) 169–179.
[53] E.H. Nicollian, J.R. Brews, MOS Physics and Technology, John Willey & Sons, New York, 1982.
[54] P. Chattopadhyay, B. Raychaudhuri, New technique for the determination of series resistance of Schottky barrier diodes, Solid-State Electron. 35 (1992) 1023–1024.
[55] A. Tataroglu, Ş. Altındal, Analysis of electrical characteristics of Au/SiO2/n-Si (MOS) capacitors using the high-low frequency capacitance and conductance methods, Microelectron. Eng. 85 (2008) 2256–2260.
[56] B. Akkal, Z. Benamara, B. Gruzza, L. Bideux, Characterization of interface states at Au/InSb/InP(100) Schottky barrier diodes as a function of frequency, Vacuum 57 (2000) 219.
[57] M. Gokcen, A. Tataroglu, Ş. Altındal, M.M. Bulbul, The effect of ^{60}Co (ɣ-ray) irradiation on the electrical characteristics of Au/SnO_2/n-Si (MIS) structures, Radiat. Phys. Chem. 77 (2008) 74–78.
[58] Ş. Karatas, A. Türüt, Ş. Altındal, Irradiation effects on the *C-V* and *G/w-V* characteristics of Sn/p-Si (MS) structures, Radiat. Phys. Chem. 78 (2009) 130–134.
[59] W.A. Hill, C.C. Coleman, A single-frequency approximation for interface-state density determination, Solid-State Electron. 23 (1980) 987.
[60] E.H. Rhoderick, R.H. Williams, Metal–Semiconductor Contacts, second ed, Clarendon, Oxford, 1988.
[61] E.H. Rhoderick, R.H. Williams, Metal-Semiconductor Contacts, Clarendon, Oxford, 1998.
[62] R.T. Tung, Recent advances in Schottky barrier concepts, Mater. Sci. Eng.: R: Rep. 35 (2001) 1–3.
[63] P. Hacke, T. Detchprohm, K. Hiramatsu, N. Sawaki, Schottky barrier on n-type GaN grown by hydride vapour phase epitaxy, Appl. Phys. Lett. 63 (1993) 2676.
[64] I. Ohdomari, K.N. Tu, Parallel silicide contacts, J. Appl. Phys. 51 (1980) 3735.
[65] J.L. Freeouf, T.N. Jackson, S.E. Laux, J.M. Woodall, Effective barrier heights of mixed phase cantacts: size effects, Appl. Phys. Lett. 40 (1982) 634.